Compressive behaviour and design of CFDST cross-sections with stainless steel outer tubes

Fangying Wang[a,*], Ben Young[b], Leroy Gardner[c]

[a] *School of Civil and Environmental Engineering, Nanyang Technological University, Singapore*
[b] *Department of Civil and Environmental Engineering, The Hong Kong Polytechnic University, Hong Kong, China. (Formerly, Department of Civil Engineering, The University of Hong Kong, Pokfulam Road, Hong Kong, China.)*
[c] *Department of Civil and Environmental Engineering, Imperial College London, London, UK*

*corresponding author. Tel.: +852 54877715
E-mail address: fangying.wang@ntu.edu.sg

Keywords: Cold-formed; Composite structures; CFDST; Design rules; Finite element modelling; Reliability analysis; Stainless steel; Structural design.

Abstract

A finite element (FE) investigation into the compressive behaviour of concrete-filled double skin tubular (CFDST) cross-sections with lean duplex and ferritic stainless steel outer tubes is presented. FE models were initially developed and validated against available test results reported in the literature. Upon successful replication of the ultimate capacities, load–deformation histories and failure modes exhibited by the tested CFDST stub columns, a parametric study was undertaken to investigate the influence of key variables, including the local slendernesses of the outer and inner tubes, the concrete strength and the adopted grade of stainless steel, on the ultimate response of the studied CFDST stub columns. Based on the generated FE data pool and the available test results, the applicability of the existing European, Australian and American design provisions for composite carbon steel members to the design of the studied CFDST cross-sections was evaluated. All the examined design rules are shown to yield unduly conservative (less so for the higher concrete grades) and rather scattered capacity predictions. Modifications to the design treatment in relation to the effective area of

the outer tubes, to take due account of outward-only local buckling, and the effective compressive strength of the infilled concrete, to reflect the reduced relative effectiveness of higher concrete grades, are considered. The modified design rules are shown to improve the accuracy and consistency of the design capacity predictions. Finally, statistical analyses were carried out to demonstrate the reliability of the modified design approaches.

1. Introduction

The use of concrete-filled steel tubular (CFST) cross-sections for compression members has become increasingly widespread in construction, owing primarily to their superior strengths, stiffnesses and ductility over plain concrete or hollow steel tubes [1,2]. The interaction between the concrete infill and the outer metal tube leads to efficient utilisation of both constituent materials by confining the concrete core and delaying local buckling of the metal tube, thereby improving the cost-effectiveness of the system. Recently, research efforts have turned towards concrete-filled double skin tubular (CFDST) cross-sections, comprising two metal tubes and sandwiched concrete filled between the tubes [3-7]. CFDST cross-sections share most of the benefits of CFST cross-sections, but will typically be lighter owing to the absence of the inner concrete core. This facilitates assembly and deconstruction and reduces foundation costs, making CFDST cross-sections an attractive choice for heavy structural applications. Such potential applications include offshore structures [3] and bridge piers [4]; an early example of the use of CFDST columns in a transmission tower is described in [5].

Stainless steel members possess a unique combination of excellent mechanical properties for structural applications and corrosion resistance, and have been utilised in construction increasingly over the past few decades [8]. An innovative form of CFDST cross-section, utilising stainless steel for the outer tube, was recently proposed [9–12], with the aim of

exploiting the most favourable properties of the constituent materials to the greatest possible extent. CFDST columns using stainless steel for the outer tubes were found to exhibit a rather more rounded and ductile load–deformation response compared to their carbon steel counterparts [10–12]. These observations mirror the findings for concrete-filled stainless steel tubular stub columns in a number of recent studies, including concrete-filled stainless steel stub columns with circular [13], rectangular [14–16] and square [14–17] cross-sections. This behaviour is directly linked to the rounded stress–strain response and substantial strain hardening that characterises stainless steel alloys. The combined advantages of the composite action seen in CFDST members, alongside the durability and ductility associated with stainless steel, make this section type potentially suitable for applications in demanding and aggressive environments, such as in offshore and marine structures, bridges and the nuclear industry.

Research into CFDST members dates back about 20 years and has mainly focussed on CFDST sections employing carbon steel tubes and sandwiched concrete grades up to 72 MPa [18]. CFDST sections with stainless steel outer tubes have been the subject of only a few studies, where their structural performance has been examined through experimentation and numerical analysis. Han et al. [9] carried out a preliminary experimental investigation to examine the behaviour of CFDST stub columns with austenitic stainless steel outer tubes. Further tests were conducted by the authors of the present paper [10] to examine the cross-sectional behaviour and resistances of CFDST stub columns with lean duplex and ferritic stainless steel outer tubes in pure compression. Meanwhile, the authors [11,12] also examined CFDST stub columns comprising austenitic stainless steel outer tubes and high strength steel inner tubes experimentally and numerically. FE analyses were employed by Hassanein and Kharoob [19] and Wang et al. [20] with the focus on CFDST cross-sections with circular hollow section (CHS) inner tubes. To date, investigations into the structural performance of CFDST members

employing stainless steel as the outer tubes have been rather limited, and the design of these members is not explicitly covered by current codes of practice. This prompted a thorough programme of research performed by the authors, aimed at examining the behaviour and capacity of CFDST structural members with stainless steel outer tubes of varying cross-section shape and devising efficient structural design rules to support their application in practice. The present paper focuses on the compressive behaviour and design of CFDST cross-sections with square or rectangular hollow section (SHS/RHS) lean duplex or ferritic stainless steel outer tubes and SHS carbon steel inner tubes.

A finite element (FE) investigation into the compressive behaviour of the examined CFDST cross-sections is reported. The numerical modelling programme comprises a validation study to replicate the structural response observed in available experiments described in the literature, and a parametric study to generate further FE data on CFDST sections of varying local slendernesses and material strengths. Based on the generated FE results, the influence of the local slendernesses of the outer and inner tubes, the concrete strength and the grade of stainless steel, on the ultimate response of the studied CFDST sections in compression is examined. The combined set of FE and test data is then adopted to assess the applicability of current design rules for concrete-filled members set out in the European Code EN 1994-1-1 (EC4) [21], Australian Standard AS5100 [22] and American Specifications AISC 360 [23] and ACI 318 [24] to the design of the studied CFDST cross-sections. Modifications to the design treatment in relation to the effective areas of the outer tubes and the effective compressive strength of the concrete are considered. Finally, the reliability of the modified design approaches is evaluated through statistical analyses.

2. Review of existing experimental data

A number of experimental investigation into the compressive behaviour of CFDST cross-sections with stainless steel outer tubes have been carried out [9–12], but the only previous experiments on CFDST cross-sections with SHS carbon steel inner tubes and SHS/RHS lean duplex and ferritic stainless steel outer tubes (see Fig. 1), which are the focus of the present study, were reported in Wang et al. [10]. In the study of Wang et al. [10], stub column tests were conducted on eight different cross-sections with lean duplex stainless steel (Grade 1.4062) RHS 150×80×3 (depth × width × thickness in mm) and SHS 100×100×3 or ferritic stainless steel (Grade 1.4003) RHS 120×80×3 and 100×80×4 as the outer tubes, and carbon steel (Grade S275) SHS 20×20×2.5, 20×20×1.5, 40×40×4 and 40×40×1.5 as the inner tubes. For each cross-section, three concrete grades with nominal concrete cylinder compressive strengths of 40, 80 and 120 MPa were employed. A total of 28 stub column tests was carried out employing the experimental rig shown in Fig. 2(a); a full description of the stub column tests is provided in Wang et al. [10]. The observed failure modes featured outward-only local buckling of the stainless steel outer tubes, crushing of the infill concrete, as well as local buckling of the carbon steel inner tube, as displayed in Fig. 3. A summary of the measured geometric and material properties, as well as the obtained experimental failure load for each stub column specimen is reported in Table 1, where D_o/t_o and D_i/t_i are the overall depth-to-thickness ratios of the outer and inner tubes respectively, in which D_o and D_i correspond to the overall depths of the outer and inner tubes, t_o and t_i are the corresponding thicknesses, $\sigma_{0.2,o}$ and $\sigma_{0.2,i}$ correspond to the material 0.2% proof stresses of the outer and inner tubes, f_c is the cylinder compressive strength of the concrete and N_{exp} is the experimental failure load.

3. Numerical modelling programme

A comprehensive numerical modelling programme was performed employing the general-purpose finite element (FE) analysis package ABAQUS [25]. FE models were established with

the aim of (i) replicating the compressive behaviour of the CFDST stub column test specimens reported in [10] and (ii) performing a parametric study to derive further FE data and investigate the influence of key variables on the structural performance of the studied CFDST cross-sections in compression. The main features of the FE models are described in Section 3.1, while the validation and parametric study are reported in Sections 3.2 and 3.3, respectively.

3.1 Development of finite element models

3.1.1. Element types and discretisation

FE models of all test specimens presented in Section 2 were established employing C3D8R [25] solid elements for the concrete and S4R [25] shell elements for the metal tubes, in line with previous numerical modelling of concrete-filled tubular members [11,12,26–29]. A systematic mesh sensitivity study was undertaken to decide upon suitable mesh settings for the FE models, in order to produce accurate yet computationally efficient results. For the cold-formed metal tubes, the element size for the flat portions was chosen to be equal to the respective cross-section thickness, while each corner of the cross-section was uniformly discretised into at least four elements to ensure a precise representation of the curved corner geometry. For the sandwiched concrete, the element sizes were selected to match those of the adjacent metal tubes in order to facilitate numerical convergence.

3.1.2. Material Modelling

The material constitutive properties of the metal tubes were represented by multi-linear elastic-plastic stress–strain curves with isotropic hardening in ABAQUS [25]. The input true stress–true plastic strain data set was derived from the measured engineering stress–strain curves, characterised by at least 100 intervals to ensure the full range of the response was accurately captured. The cold-formed metal tubes experienced plastic deformations during the cold-rolling

process, causing an increase in strength and a loss in ductility. This is particularly pronounced in the corner regions and more significant in stainless steel, as observed from the coupon test results reported by Wang et al. [10]. The yield strengths of the corner materials were found to be about 50%, 35% and 10% higher, on average, than those of the flat materials for the lean duplex stainless steel, ferritic stainless steel, and carbon steel sections, respectively. Hence, allowance for this was made in the current FE models by assigning the corner material properties to the respective curved corner regions and the adjacent flat regions beyond the corners by a distance of two times the cross-section thickness, following the recommendations of [30].

The material properties of the sandwiched concrete were characterised by the built-in concrete damage plasticity (CDP) model in ABAQUS [25]. The Poisson's ratio of the concrete and modulus of elasticity E_c were set respectively equal to 0.2 and $4733\sqrt{f_c}$, respectively, in accordance with ACI 318 [24]. For the compressive properties of the concrete used in the CDP model, a confined concrete stress–strain curve was adopted to take due account of the confinement afforded to the concrete by the metal tubes. The confined stress–strain curve was originally calibrated against test data on carbon steel CFST stub columns with concrete cylinder compressive strengths ranging from 13 to 164 MPa by Tao et al. [28], and modified by the authors [11,12] for application to CFDST stub columns with stainless steel outer tubes. The modifications were concerned primarily with the confinement factor (ξ_c), as defined by Eq. (1),

$$\xi_c = \frac{A_o \sigma_{0.2,o}}{A_{ce} f_c} \tag{1}$$

where A_o is the cross-sectional area of the outer tube and A_{ce} is an equivalent cross-sectional area of the sandwiched concrete, defined as the full area enclosed by the outer tube, as given by Eq. (2), where $r_{int,o}$ is the internal corner radius of the outer tube.

$$A_{ce} = (D_o - 2t_o)^2 - (4 - \pi) r_{int,o}{}^2 \quad (2)$$

For the tensile properties of the concrete used in the CDP model, a stress–strain curve comprising a linear response up to the ultimate tensile strength, taken as $0.1f_c$, and a descending branch characterised by fracture energy (G_F) [25,28], was adopted throughout the numerical modelling programme.

3.1.3. Boundary conditions and interactions

The geometry, loading and experimentally observed failure modes of the studied CFDST specimens were doubly symmetric. Hence, to enhance computational efficiency, only one-quarter of the cross-sections and half of the stub column lengths were modelled, with suitable boundary conditions assigned to the planes of symmetry, as depicted in Fig. 2(b). For ease of application of boundary conditions, the end sections of the three constituent parts of the CFDST stub columns were coupled to three reference points, which were restrained against all degrees of freedom except longitudinal translation in order to attain fixed-ended boundary conditions. The same value of longitudinal displacement was applied at the three reference points to mimic the displacement-controlled compressive loading scheme used in the experiments.

The interaction between the outer and inner tubes and the concrete was modelled using surface-to-surface contact. “Hard contact” was employed in the normal direction, while the Coulomb friction model was adopted to simulate the tangential behaviour. A value of 0.6 was selected for the friction coefficient, though a prior sensitivity study had revealed that the compressive response of the studied CFDST cross-sections was relatively insensitive to variation in this parameter [31]. This is primarily due to the nature of the loading (i.e. axial compression), under which the slip at the interfaces was negligible since the concrete and the metal tubes largely deform together.

3.1.4. Initial imperfections and residual stresses

Local geometric imperfections and residual stresses have negligible influence on the behaviour of CFDST stub columns, owing principally to the fact that (i) the lateral pressure applied to the steel tubes from the expansion of the concrete obviates the need to assign any geometric perturbation to induce local buckling, and (ii) the support afforded to the metal tubes by the concrete lessens the sensitivity of the tubes to local instabilities [11,12]. Therefore, local geometric imperfections and residual stresses were not explicitly included in the current FE models. The suitability of this treatment is confirmed through the validation of the FE models reported in Section 3.2.

3.1.5. Solution schemes

The modified Riks method (Riks) is commonly adopted for solving static numerical problems with geometrical and material nonlinearities [25], and was generally employed in the present study for the displacement-controlled nonlinear numerical analyses of the CFDST stub columns. However, for some of the models, particularly those with more slender metal tubes, convergence problems inhibited attainment of the peak loads or tracing of the post-ultimate responses In these cases, an adaptive automatic stabilisation scheme [25], which allows the model to be stabilised by implementing an artificial viscous damping force, was employed in the FE simulations. This approach has been successfully utilised for cold-formed steel members and systems in [32,33], and shown to achieve satisfactory results provided that a sufficient number of increments are achieved before the peak load is reached and that the ratio of the energy dissipated by viscous damping (ALLSD) to the total strain energy (ALLIE) remains low. In this study, at least 50 successful increments prior to reaching the peak load were achieved

and the ratios of ALLSD/ALLIE remained below 2%. The load versus average axial strain (defined as the axial shortening divided by the stub column length) curve obtained using the automatic stabilisation scheme is compared with that obtained using the modified Riks method in Fig. 4 for a typical FE model featuring an SHS 600×600×12 lean duplex outer tube, an SHS 300×300×5 carbon steel inner tube and a concrete strength of 40 MPa; this specimen is denoted LS600×12-NS300×5-C40 herein. The comparison reveals that similar results are achieved using the two solution schemes with a maximum discrepancy of approximately 1% at the peak load.

3.2. Validation of FE model

The developed FE model was validated with reference to the results of the tested CFDST stub columns presented in Section 2; comparisons were made of the ultimate loads, load–displacement curves and failure modes. Table 1 reports the numerical to experimental ultimate compressive capacity ratio (N_{FE}/N_{exp}) for each tested CFDST specimen. A mean value of N_{FE}/N_{exp} of 1.02 with a coefficient of variation (COV) of 0.035 was achieved, indicating that the FE ultimate strengths are in close agreement with those obtained from the tests. The FE models were also found to reproduce accurately the full load–deformation histories of the respective stub column tests, examples of which are displayed in Fig. 5. The exhibited failure modes were also well replicated numerically, as shown in Fig. 3. Overall, it may be concluded that the established FE models can accurately and reliably simulate the experimental structural responses of the examined CFDST stub columns.

3.3. Parametric study

The successfully validated FE models were utilised to acquire further FE data on CFDST cross-sections with varying cross-section slendernesses and material strengths. The CFDST cross-

sections included in the parametric study cover compact, noncompact and slender cross-sections, with reference to the classification limits for composite cross-sections in AISC 360 [23]. Regarding the geometric properties of the modelled cross-sections, the inner and outer tubes were SHS with overall widths fixed at 300 and 600 mm, respectively, while the thicknesses were varied to generate a wide spectrum of local slenderness values (d_i/t_i and d_o/t_o) from 6 to 146, where d_i and d_o are the flat element widths of the inner and outer tubes. Note that the studied d_o/t_o ratios cover the practical range of available rolled stainless steel sections but also extend to more slender sections, which could be produced by press-braking, to assess their performance in concrete-filled tubular construction. The internal corner radii of the outer and inner tubes were set equal to the respective section thicknesses. The length of each FE model was equal to $2.5D_o$, mirroring the test specimens. Throughout the parametric study, the measured material properties of the tested lean duplex stainless steel SHS 100×100×3 and ferritic stainless steel RHS 120×80×3 were used for the outer tubes, while those of the tested carbon steel SHS 40×40×4 were used for the inner tubes. Three concrete grades with concrete compressive strengths of 40, 80 and 120 MPa were adopted. Table 2 lists the ranges of variation of the aforementioned parameters considered herein. Overall, a total of 311 CFDST specimens was simulated in the parametric study.

The derived FE results were employed to examine the influence of the key variables on the ultimate strength of the studied CFDST stub columns (N_u), including the local slendernesses of the outer and inner tubes, the concrete grade and the stainless steel grade. Note that the load–axial strain curves for some compact specimens did not reach their peak loads despite large plastic deformations. For these specimens, the ultimate strength was defined as the load at which the tangent stiffness of the load–axial strain curve at increment i, K_i, reached 1% of its initial stiffness, K_{ini} — i.e. failure was taken at the point when $K_i/K_{ini} = 0.01$, a typical example

of which is illustrated in Fig. 6. This approach was proposed by dos Santos et al. [34] and has been employed for the definition of the ultimate strengths of concrete-filled tubular members in [11,12,14].

3.3.1 Influence of local slenderness of metal tube

The influence of the local slenderness of the outer tube on the ultimate response is assessed through comparisons among specimens with the same inner tubes and concrete grades but varying local slenderness values for the outer tube (d_o/t_o). In the comparisons presented, the ultimate strength (N_u) obtained from the CFDST stub column FE simulations are normalised by the respective plastic strength (N_{pl}) of the cross-sections, as defined by Eq. (3), which is a simple summation of the plastic resistances of the outer tube, concrete and inner tube.

$$N_{pl} = A_o\sigma_{0.2,o} + A_c f_c + A_i\sigma_{0.2,i} \tag{3}$$

The results are displayed in Fig. 7, where the normalised strength (N_u/N_{pl}) is plotted against the local slenderness of the outer tube d_o/t_o. A total of 10 groups of data, differentiated by the local slenderness of inner tube d_i/t_i, are compared, each comprising a spectrum of d_o/t_o ratios ranging from 4 to 146. It can be observed that the specimens with the more compact outer tubes exhibited the higher values of N_u/N_{pl}; this is attributed to the reduced susceptibility to local buckling and the improved confinement afforded to the concrete. Typical load–axial strain curves, shown for specimens LS600×5-NS300×10-C40, LS600×20-NS300×10-C40 and LS600×30-NS300×10-C40, are presented in Figs 8(a)–(c), while the load–carrying contributions from the outer tube, concrete and inner tube, normalised by their corresponding plastic loads (denoted $A_o\sigma_{0.2,o}$, A_cf_c and $A_i\sigma_{0.2,i}$), are compared in Figs 8(d)–(f). It can be seen that the slender stainless steel outer tube (LS600×5) was prone to local buckling and failed to attain its yield load ($A_o\sigma_{0.2,o}$), while the more compact outer tubes (LS600×20 and LS600×30)

were able to exceed their yield loads and exhibit the pronounced strain hardening that characterises stainless steel materials. The performance of the sandwiched concrete, in terms of both strength and ductility, was also found to improve when a more compact outer tube was used due to the greater confinement afforded to the concrete, as depicted in Fig 8(e).

Compared to the local slenderness of the outer tube, that of the inner tube was found to be less influential on the ultimate response of the studied CFDST cross-sections. This can be seen in Fig. 7, where, for a given d_o/t_o value, the difference in results between the CFDST stub columns with varying d_i/t_i values is minimal. This is also evident in Fig. 9, where the normalised strength N_u/N_{pl} can be seen to remain almost unaltered across the range of d_i/t_i ratios from 6 to 146. Typical examples are shown in Fig. 10 for the examined CFDST stub columns with d_i/t_i ratios of 26, 56 and 96. It can be seen that the performance of the outer tube and concrete appears not to be greatly influenced by the compactness of the inner tube; in addition, despite the inner tube failing by local buckling at a relatively low average axial strain for specimen LS600×3-NS300×3-C40, the ultimate strength of the cross-section, which is dominated by the outer tube and the concrete, is reached at a much later stage. Overall, it is concluded that the compactness of the stainless steel outer tube has a substantial influence on the ultimate response of the CFDST cross-sections, while the local slenderness of the carbon steel inner tube, which represents only a relatively small contribution to the plastic resistance of the overall CFDST cross-section, is less influential.

3.3.2 Influence of concrete grade

Three concrete grades were assessed in the parametric study, with nominal compressive concrete strengths of 40, 80 and 120 MPa. The confined strength of the concrete is directly linked to the cross-sectional compactness and is mainly governed by the local slenderness of

the outer tube. Comparisons of normalised strength (N_u/N_{pl}) were therefore made with respect to the local slenderness of the outer tube (d_o/t_o), as shown in Fig. 11. It can be seen that the lower concrete grades result in better normalised ultimate performance in the case of lower outer tube slenderness values, revealing that lower concrete grades can benefit to a greater extent from the confinement offered by the outer tube, provided that the tube is sufficiently stocky.

3.3.3 Influence of stainless steel grade

Two stainless steel grades, lean duplex stainless steel (Grade 1.4062) and ferritic stainless steel (Grade 1.4003), were examined in this study. The ultimate performance of CFDST cross-sections utilising the two different grades of stainless steel for the outer tube are compared in Fig. 12(a), revealing improved structural performance associated with the use of the lean duplex grade, particularly in the case of the more compact outer tubes. This is attributed to the more pronounced strain hardening and higher ductility of lean duplex stainless steel over ferritic stainless steel, as displayed in Fig. 12(b).

4. Evaluation of current international design codes

4.1 General

The applicability of the European Code EN 1994-1-1 (EC4) [21], the Australian Standard AS 5100 [22] and the two American Specifications—AISC 360 [23] and ACI 318 [24] for composite carbon steel members to the design of the studied CFDST cross-sections is appraised in this section. Limitations on cross-sectional slenderness and material strengths specified in the examined codes are summarised in Table 3. Note that although these code limitations are exceeded for some of the tested [10] and modelled stub columns, comparisons and evaluations

are still presented to explore possible extension of the codes beyond their current range applicability.

4.2 European Code EN 1994-1-1 (EC4)

The design expression for the axial compressive resistances of square or rectangular carbon steel CFST cross-sections in EC4 [21] is a summation of the plastic resistance of the metal tubes and concrete infill. Account is taken of the higher strength of the concrete infill as a result of the confinement provided by the outer tube, by implementing a concrete coefficient of 1.0, rather than 0.85. The analogous cross-section capacity (N_{EC4}) for a concrete-filled square or rectangular CFDST cross-section in compression is thus given by Eq. (4).

$$N_{EC4} = A_o \sigma_{0.2,o} + A_c f_c + A_i \sigma_{0.2,i} \tag{4}$$

A slenderness limit of $D_o/t_o \leq 52(235/f_y)^{0.5}$ for concrete-filled composite members is defined in EC4 [21], beyond which the effects of local buckling need to be considered. In this study, this slenderness limit is slightly modified to reflect the difference in Young's modulus between stainless steel and carbon steel, thus: $D_o/t_o \leq 52\sqrt{(235/\sigma_{0.2,o})(E_o/210000)}$. For the CFDST cross-sections exceeding this modified slenderness limit, the effective width formulation set out in EN 1993-1-4 [35,36] for slender stainless steel internal plate elements, as given by Eq. (5), was used for calculating the effective area of the outer tube, where ρ is the local buckling reduction factor, and $\bar{\lambda}_p$ is the plate element slenderness and can be determined from Eq. (6), in which v is the Poisson's ratio, taken as 0.3, E_o is the Young's modulus of the outer tube, and k is the buckling coefficient, taken equal to 4 for plates with simply supported boundary conditions in pure compression [37,38].

$$\rho = \frac{0.772}{\bar{\lambda}_p} - \frac{0.079}{\bar{\lambda}_p^{\,2}} \tag{5}$$

$$\bar{\lambda}_p = \sqrt{\frac{\sigma_{0.2,o}}{\sigma_{cr}}} = \sqrt{\frac{12(1-\upsilon^2)\sigma_{0.2,o}}{k\pi^2 E_o}}(d_o/t_o) \quad (6)$$

4.3 Australian Standard AS 5100

The Australian Standard AS 5100 [22] adopts the same approach to obtain the axial compressive design resistances as given in EC4 [21], but with a different slenderness limit and effective width expression. A yield slenderness limit of 40 is specified for the flat faces of the outer tube (λ_e) in AS 5100, where the local slenderness λ_e was also modified for stainless steel, as given by $(d_o/t_o)(\sigma_{0.2,o}/250)^{0.5}$. For the design strengths of the test specimens and FE models that exceed this limit, effective areas were again used in place of the gross areas to account for local buckling. The effective width expression for cold-formed stainless steel tubular cross-sections set out in AS/NZS 4673 [39] was adopted for the comparisons with the Australian design provisions, as given by Eq. (7), where λ is a local slenderness, as given by Eq. (8), in which F_n is the overall buckling stress of the column, equal to $\sigma_{0.2,o}$ due to the short length of the studied stub columns, and k is again taken as 4 according to AS/NZS 4673 [39]. Hence, the slenderness λ is essentially the same as that employed in EN 1993-1-4 [35], denoted $\bar{\lambda}_p$ and defined by Eq. (5).

$$\rho = \frac{1-0.22/\lambda}{\lambda} \quad (7)$$

$$\lambda = \left(\frac{1.052}{\sqrt{k}}\right)\frac{d_o}{t_o}\left(\sqrt{\frac{F_n}{E_o}}\right) \quad (8)$$

4.4 American design provisions AISC 360 and ACI 318

The AISC 360 compressive cross-section strength (N_{AISC}) for a square or rectangular concrete-filled column is presented as a function of the slenderness (compactness) of the flat faces of the steel section ($\lambda=d_o/t_o$), as determined from Eq. (9),

400
$$N_{AISC} = \begin{cases} A_o\sigma_{0.2,o} + 0.85A_c f_c + A_i\sigma_{0.2,i} & (\lambda < \lambda_p) \\ P_p - \dfrac{P_p - P_y}{\left(\lambda_r - \lambda_p\right)^2}\left(\lambda - \lambda_p\right)^2 + A_i\sigma_{0.2,i} & (\lambda_p \le \lambda < \lambda_y) \\ A_o f_{cr} + 0.7A_c f_c + A_i\sigma_{0.2,i} & (\lambda \ge \lambda_y) \end{cases} \quad (9)$$

401 where P_p and P_y are determined from Eq. (10) and (11) respectively, λ_p and λ_r correspond to
402 the limits between compact/noncompact and noncompact/slender cross-sections, again
403 modified for stainless steel herein, given by $2.26(E_o/\sigma_{0.2,o})^{0.5}$ and $3.00(E_o/\sigma_{0.2,o})^{0.5}$ respectively,
404 and f_{cr} is the elastic critical local buckling stress of the outer tube, as given by Eq. (12). Note
405 that the contribution from the inner tube in the resistance function is treated as an independent
406 term, rather than a concrete dependent term as for reinforcing bars; further explanation has been
407 provided in previous work by the authors [10–12].

408
$$P_p = A_o\sigma_{0.2,o} + 0.85A_c f_c + A_i\sigma_{0.2,i} \quad (10)$$

409
$$P_y = A_o\sigma_{0.2,o} + 0.7A_c f_c + A_i\sigma_{0.2,i} \quad (11)$$

410
$$f_{cr} = \frac{9E_o}{\left(d_o/t_o\right)^2} \quad (12)$$

411 The American Concrete Institute design provisions for CFST cross-sections, as set out in ACI
412 318 [24], are also assessed herein. The confinement afforded to the concrete from the steel tube
413 is not explicitly considered in ACI 318. Hence, the cross-section resistance (N_{ACI}) is given by
414 Eq. (13).

415
$$N_{ACI} = A_o\sigma_{0.2,o} + 0.85A_c f_c + A_i\sigma_{0.2,i} \quad (13)$$

416 The gross area of the outer tube may be used in Eq. (13) provided that the tube thickness satisfies
417 $t_o \ge D_o(\sigma_{0.2,o}/3E_o)^{0.5}$ [24]. For the design strengths of the test and FE specimens outside this
418 range, effective areas were again used in place of the gross areas to account for local buckling,
419 and the effective width expression for cold-formed stainless steel tubular cross-sections given
420 in the SEI/ASCE-8-02 [40] was utilised in the calculations. Note that SEI/ASCE-8-02 [40]
421 employs the same effective width formulation as AS/NZS 4673 [40], as given by Eq. (7).

4.5 Assessment of current design methods

In this section, the accuracy of the predicted cross-section compressive strengths from the described design methods is evaluated by comparisons against the test and FE failure loads. The mean test and FE to design code prediction ratios N_u/N_{code}, as presented in Table 4, are respectively equal to 1.20, 1.17, 1.27, and 1.27 for EC4, AS 5100, AISC 360 and ACI 318, with COVs of 0.108, 0.100, 0.131, and 0.086, revealing that the current design rules result in rather conservative and scattered compressive strength predictions for the studied CFDST cross-sections. The high level of conservatism and scatter is also evident in Figs 13–16, where the ratios of N_u/N_{code} are plotted against the normalised cross-section slenderness (λ) of each examined code, together with the corresponding normalised cross-section slenderness limits; a summary of the normalised cross-section slenderness measures and limits is reported in Table 3. It can be seen that the predictions for the CFDST cross-sections falling within the slenderness limits are unduly conservative, especially in the lower cross-section slenderness range, which may be attributed to the lack of consideration for the substantial strain hardening that the stainless steel outer tube exhibits and the higher degree of confinement afforded to the concrete infill from the stockier outer tubes.

5. Modifications to design rules

5.1 Modification to high strength concrete

The results from the parametric analyses have revealed that the degree of influence of the concrete strength on the compressive capacities of the studied CFDST stub columns differs among the concrete grades, particularly for CFDST stub columns with compact outer tubes. It is therefore suggested that this difference is reflected in the design formulations. It can also be seen in Table 5 that the accuracy of the compressive strength predictions varies with concrete

grade for all the examined design codes. Specifically, the design predictions of CFDST cross-sections with lower grade concrete were found to be more conservative than their counterparts with higher grade concrete. This observation echoes the experimental results for the studied CFDST cross-sections in [10], and also mirrors the findings for CFST cross-sections [14] and other CFDST cross-sections [11,12]. To address this, it is proposed that the concrete strength (f_c) in the design expressions is modified by multiplying by a reduction factor η, as specified in EN 1992-1-1 [41] and given by Eq. (14), to account for the effective compressive strength of high grade concrete (greater than 50 MPa). Note that the reduction factor η in EN 1992-1-1 [41] only covers concrete strengths up to 90 MPa, beyond which a constant value of 0.8, as proposed by Liew et al. [42], is employed herein.

$$\eta = 1.0 - \frac{f_c - 50}{200} \tag{14}$$

The accuracy of the modified capacity predictions is assessed in Table 5, where the mean test and FE to design code prediction ratios (N_u/N_{EC4*}, $N_u/N_{AS5100*}$, N_u/N_{AISC*}, and N_u/N_{ACI*}) and the corresponding COVs for the three concrete grades are presented. The results from the assessment reveal that with the inclusion of the reduction factor η, the modified capacity predictions are more consistent and less scattered across the range of concrete grades from C40 to C120.

5.2 Modification to design of steel tube

The existing design codes were generally found to result in excessively conservative compressive capacity predictions for the CFDST cross-sections exceeding the specified code slenderness limits. This is can be primarily attributed to the neglect of the beneficial restraining effect of the concrete on the local buckling of the stainless steel outer tubes. Unlike in hollow SHS/RHS members, the local buckling failure mode of the outer tube in the examined CFDST cross-sections features outward-only deformation of all four faces, rather than alternating

inward and outward deformations of adjacent faces. It has been shown that the elastic buckling coefficient k [37,38] increases from 4 for conventional (two-way) local buckling of uniformly compressed simply-supported plates to 10.67 for outward-only local buckling [43]. A modified local buckling coefficient k equal to 10.67, rather than 4, has therefore been employed by the authors [10,12] in previous studies to reflect the restraining effect of the concrete on the local buckling of the stainless steel outer tubes. This approach is also assessed herein in the implementation of the design rules in EC4, AS 5100 and ACI 318, taking the local buckling coefficient k as 10.67 in calculating the plate slenderness and hence the effective areas of the outer tubes. It is worth noting that due account of the outward-only buckling mode has already been taken in AISC 360 [23] and reflected in the cross-section noncompact slenderness limit [44,45], which is derived by factoring the corresponding limit for hollow steel cross-sections, $1.40(E/F_y)^{0.5}$, by a value of $(10.67/4)^{0.5}$; further explanation is provided in previous work by the authors [10].

Quantitative comparisons of the compressive capacities predicted by the modified EC4, AS 5100 and ACI 318 (N_{code*}) incorporating the higher buckling coefficient k of 10.67, and the corresponding predictions from the unmodified design rules with k=4, with test and FE ultimate strengths are reported in Table 6 for the slender CFDST cross-sections that fall outside the respective codified noncompact slenderness limits. The mean ratios of N_u/N_{code*} are all closer to unity and less scattered than those for the case of k=4. The notably improved accuracy and consistency is also evident in the graphical comparisons presented in Figs 13, 14 and 16, respectively for the modified EC4, AS 5100 and ACI 318 predictions.

5.3 Reliability analysis and discussion

Statistical analyses were conducted to assess the reliability associated with the application of the current and modified design rules to the examined CFDST cross-sections, according to the procedures and requirements specified in EN 1990 [46]. In the present analyses, the mean to nominal yield strength ratios $f_{y,mean}/f_{y,nom}$ were taken as 1.10 [47], 1.20 [47], and 1.16 [48], with COVs of 0.030 [47], 0.045 [47] and 0.055 [48] for the lean duplex stainless steel, ferritic stainless steel and the carbon steel, respectively. For the sandwiched concrete, the over-strength ratio was determined from Eq. (15) [49],

$$f_c = f_m - 1.64\delta \tag{15}$$

where f_m is the mean compressive concrete strength, and δ is the standard deviation, derived from the measured COV values 0.019, 0.005 and 0.029 for C40, C80 and C120, respectively [10]. The concrete over-strength ratios were therefore equal to 1.03, 1.01 and 1.05 for C40, C80 and C120, respectively, while the COV of the concrete strengths used in the reliability analysis was conservatively taken as 0.180 [49] for all grades. The COVs of the geometric properties of the stainless steel outer tube, concrete and carbon steel inner tube were taken as 0.05 [47], 0.01 [50] and 0.03 [48], respectively. Note that the partial factors for stainless steel, concrete and carbon steel were taken as 1.10 [35], 1.50 [41] and 1.00 [51] in the assessment of the European design provisions, while corresponding values of 1.11, 1.67 and 1.11 were used in the assessment of the Australian design provisions, converted (inverted) from resistance factors of 0.9, 0.6 and 0.9 prescribed in AS 5100 [22] in the numerator rather than denominator. American specifications consider the overall resistance factors, rather than individual partial factors in composite design, with current recommended values in the numerator 0.75 and 0.65 for concrete-filled tubular members, as specified in AISC 360 [23] and ACI 318 [24], respectively. Therefore, the target partial safety factors for composite sections are equal to 1.0 for EC4 and

AS5100 design provisions since the individual target partial factors described above are already included, and 1.33 and 1.54 for AISC 360 and ACI 318, respectively.

The key parameters and results from the Eurocode reliability analysis are summarised in Table 7, where $k_{d,n}$ is the design fractile factor, b is the average ratio of experimental and numerical capacities to design model capacities [52], V_δ is the COV of the experimental and numerical simulations relative to the resistance model, and γ_{M0} is the resulting partial safety factor for the compressive strengths of the studied CFDST cross-sections. As can be seen from Table 7, the required partial factors for the original and modified design rules are all close to or less than the target values, and thus both the current and modified design rules are considered to satisfy the reliability requirements of EN 1990 [46].

6. Conclusions

A comprehensive numerical modelling programme undertaken to examine the compressive behaviour of CFDST cross-sections with lean duplex and ferritic stainless steel outer tubes is reported in this paper. Finite element models have been established to replicate test results reported in the literature, and utilised to acquire further FE data through parametric analyses. The influence of key parameters on the ultimate response of the studied CFDST stub columns was examined, including the local slendernesses of the outer and inner tubes, the concrete strength and the stainless steel grade. The results of the parametric study generally revealed that (i) the compactness of the stainless steel outer tube has a substantial influence on the ultimate response of the CFDST cross-sections, while the local slenderness of the carbon steel inner tube is less influential; (ii) the lower concrete grades can benefit to a greater extent from the confinement offered by the outer tube; (iii) the use of lean duplex grade rather than ferritic stainless steel for the outer tube results in superior CFDST compressive performance. Based on

544 the test and FE results, the applicability of the European Code EN 1994-1-1 (EC4) [21], the
545 Australian Standard AS 5100 [22] and the two American Specifications—AISC 360 [23] and
546 ACI 318 [24] for composite carbon steel members to the design of the studied CFDST cross-
547 sections was assessed. The assessment results generally indicated that the existing design rules
548 result in safe-sided, but unduly conservative (less so for the higher concrete grades) and rather
549 scattered capacity predictions.
550

551 Inaccuracies in the compressive resistance predictions stemmed principally from the lack of
552 consideration of strain hardening in the stainless steel outer tubes, insufficient allowance for
553 the restraining effect of the concrete against local buckling of the metal tubes and differences
554 in behaviour between high strength and normal strength concrete not being fully recognised.
555 Modifications to the current design provisions were therefore considered— a reduction factor
556 η to reflect the reduced relative effectiveness of using higher concrete grades and a higher
557 buckling coefficient k of 10.67 to consider the beneficial restraining effect of the concrete on
558 the local buckling of the stainless steel outer tubes. The modified design rules are shown to
559 yield greater accuracy and consistency, and their reliability was confirmed through statistical
560 analyses.
561

562 **Acknowledgements**

563 The authors are grateful to Mr. Cheuk Him Wong for his assistance in the experimental program
564 as part of his final year undergraduate research project at the University of Hong Kong. The
565 authors are grateful to STALA Tube Finland for supplying the test specimens.
566

567 **References**

[1] T.M. Chan, L. Gardner, K.H. Law, Structural design of elliptical hollow sections: a review, Proc. Inst. Civ. Eng. Struct. Build. 163(6) (2010) 391–402.

[2] L.-H. Han, W. Li, R. Bjorhovde, Developments and advanced applications of concrete-filled steel tubular (CFST) structures: Members, J. Constr. Steel Res. 100 (2014) 211–228.

[3] S. Wei, S. Mau, C. Vipulanandan, S. Mantrala, Performance of new sandwich tube under axial loading: experiment, ASCE J. Struct. Eng. 121(12) (1995) 1806–1814.

[4] K. Nakanishi, T. Kitada, H. Nakai, Experimental study on ultimate strength and ductility of concrete filled steel columns under strong earthquake, J. Constr. Steel Res. 51(3) (1999) 297–319.

[5] W. Li, Q.-X. Ren, L.-H. Han, X.-L. Zhao, Behaviour of tapered concrete-filled double skin steel tubular (CFDST) stub columns, Thin-Walled Struct. 57 (2012) 37–48.

[6] X.-L. Zhao, L.-W. Tong, X.-Y. Wang, CFDST stub columns subjected to large deformation axial loading, Eng. Struct. 32(3) (2010) 692–703.

[7] F. Zhou, B. Young, Compressive strengths of concrete-filled double-skin (circular hollow section outer and square hollow section inner) aluminium tubular sections, Adv. Struct. Eng. 22(11) (2019) 2418–2434.

[8] L. Gardner, Stability and design of stainless steel structures – Review and outlook, Thin-Walled Struct. 141 (2019) 208–216.

[9] L.-H. Han, Q.-X. Ren, W. Li, Tests on stub stainless steel–concrete–carbon steel double-skin tubular (DST) columns, J. Constr. Steel Res. 67(3) (2011) 437–452.

[10] F. Wang, B. Young, L. Gardner, Experimental study of CFDST sections with stainless steel SHS and RHS outer tubes under axial compression, ASCE J. Struct. Eng. 145(11) (2019) 04019139.

[11] F. Wang, B. Young, L. Gardner, Compressive testing and numerical modelling of concrete-filled double skin CHS with austenitic stainless steel outer tubes, Thin-Walled Struct. 141 (2019) 345–359.

[12] F. Wang, B. Young, L. Gardner, CFDST sections with square stainless steel outer tubes under axial compression: Experimental investigation, numerical modelling and design, Eng. Struct. 207 (2020) 110189.

[13] D. Lam, L. Gardner, Structural design of stainless steel concrete filled columns, J. Constr. Steel Res. 64(11) (2008) 1275–1282.

[14] A. He, F. Wang, O. Zhao, Experimental and numerical studies of concrete-filled high-chromium stainless steel tube (CFHSST) stub columns, Thin-Walled Struct. 144 (2019) 106273

[15] B. Uy, Z. Tao, L.-H. Han, Behaviour of short and slender concrete-filled stainless steel tubular columns, J. Constr. Steel Res. 67(3) (2011) 360–378.

[16] B. Young, E. Ellobody, Experimental investigation of concrete-filled cold-formed high strength stainless steel tube columns, J. Constr. Steel Res. 62(5) (2006) 484–492.

[17] Q.-H. Tan, L. Gardner, L.-H. Han, T.-Y. Song, Fire performance of steel reinforced concrete-filled stainless steel tubular (CFSST) columns with square cross-sections, Thin-Walled Struct. 143 (2019) 106197.

[18] F. Wang, B. Young, L. Gardner, Experimental investigation of concrete-filled double skin tubular stub columns with stainless steel outer tubes. Proc. 8th Int. Conf. Steel Aluminium Struct., Hong Kong, China, paper 118 (2016).

[19] M.F. Hassanein, O.F. Kharoob, Analysis of circular concrete-filled double skin tubular slender columns with external stainless steel tubes, Thin-Walled Struct. 79 (2014) 23–37.

[20] F.-C. Wang, L.-H. Han, W. Li, Analytical behavior of CFDST stub columns with external stainless steel tubes under axial compression, Thin-Walled Struct. 127 (2018) 756–768.

[21] European Committee for Standardisation (CEN), EN 1994-1-1:2004 Eurocode 4: Design of Composite Steel and Concrete Structures – Part 1-1: General Rules and Rules for Buildings, 2004.

[22] Standards Australia, AS5100.6-2004 Bridge Design, Part 6: Steel and Composite Construction, 2004.

[23] American Institute of Steel Construction, ANSI/AISC 360-16 Specification for Structural Steel Buildings, 2016.

[24] American Concrete Institute, ACI 318-14 Building Code Requirements for Structural Concrete and Commentary, 2014.

[25] Karlsson Hibbitt, Sorensen, Inc. ABAQUS, ABAQUS/Standard User's Manual Volumes I–III and ABAQUS CAE Manual. Version 6.12 Pawtucket (USA) 2012.

[26] A. He, Y. Liang, O. Zhao, Behaviour and residual compression resistances of circular high strength concrete-filled stainless steel tube (HCFSST) stub columns after exposure to fire, Eng. Struct. 203 (2020) 109897.

[27] A. Espinos, L. Gardner, M. Romero, A. Hospitaler, Fire behaviour of concrete-filled elliptical steel columns, Thin-Walled Struct. 49 (2) (2011) 239–255.

[28] Z. Tao, Z.B. Wang, Q. Yu, Finite element modelling of concrete-filled steel stub columns under axial compression. J. Constr. Steel Res. 89 (2013) 121–131.

[29] A. He, O. Zhao, Experimental and numerical investigations of concrete-filled stainless steel tube stub columns under axial partial compression, Journal of Constructional Steel Research 158 (2019) 405–416.

[30] R.B. Cruise, L. Gardner L. Strength enhancements induced during cold forming of stainless steel sections, J. Constr. Steel Res. 64(11) (2008) 1310–1316.

[31] Wang F. Behaviour and design of concrete-filled double skin stainless steel members. PhD thesis, Department of Civil engineering, the University of Hong Kong, Hong Kong, China; 2018.

[32] B.W. Schafer, Z. Li, C.D. Moen, Computational modeling of cold-formed steel, Thin-Walled Struct. 48(10-11) (2010) 752-762.

[33] P. Kyvelou, L. Gardner, D.A. Nethercot, Finite element modelling of composite cold-formed steel flooring systems, Eng. Struct. 158 (2018) 28-42.

[34] G.B. dos Santos, L. Gardner, M. Kucukler, A method for the numerical derivation of plastic collapse loads, Thin-Walled Struct 124 (2018) 258-277.

[35] European Committee for Standardisation (CEN), EN 1993-1-4:2006 Eurocode 3: Design of Steel Structures – Part 1.4: General Rules –Supplementary Rules for Stainless Steels, 2006.

649 [36] L. Gardner, M. Theofanous, Discrete and continuous treatment of local buckling in stainless
650 steel elements, J. Constr. Steel Res. 64(11) (2008) 1207-1216.
651 [37] European Committee for Standardisation (CEN), EN 1993-1-5:2006 Eurocode 3: Design of
652 Steel Structures – Part 1-5: General rules - Plated structural elements, 2006.
653 [38] L. Gardner, A. Fieber, L. Macorini, Formulae for calculating elastic local buckling stresses of
654 full structural cross-sections, Struct. 17 (2019) 2-20.
655 [39] Standards Australia, AS/NZS 4673-2001 Cold-formed Stainless Steel Structures, 2001.
656 [40] American Society of Civil Engineers (ASCE), SEI/ASCE 8-02 Specification for the Design of
657 Cold-formed Stainless Steel Structural Members, 2002.
658 [41] European Committee for Standardization (CEN), EN 1992-1-1:2004 Eurocode 2: Design of
659 Concrete Structures-Part 1-1: General Rules and Rules for Buildings, 2004.
660 [42] J.Y.R. Liew, M. Xiong, D. Xiong, Design of Concrete Filled Tubular Beam-columns with High
661 Strength Steel and Concrete, Struct. 8 (2016) 213-226.
662 [43] B. Uy, M.A. Bradford, Elastic local buckling of steel plates in composite steel-concrete
663 members, Eng. Struct. 18(3) (1996) 193-200.
664 [44] Z. Lai, A.H. Varma, K. Zhang, Noncompact and slender rectangular CFT members:
665 Experimental database, analysis, design, J. Constr. Steel Res. 101 (2014) 455-468.
666 [45] R.T. Leon, D.K. Kim, J.F. Hajjar, Limit state response of composite columns and beam-columns
667 part 1: Formulation of design provisions for the 2005 AISC specification, Eng. J. AISC 44(4)
668 (2007) 341.
669 [46] EN 1990, Eurocode 0: basis of structural design. Brussels: European Committee for
670 Standardization (CEN), 2008.
671 [47] S. Afshan, P. Francis, N.R. Baddoo, L. Gardner, Reliability analysis of structural stainless steel
672 design provisions, J. Constr. Steel Res. 114 (2015) 293-304.
673 [48] M. Byfield, D. Nethercot, Material and geometric properties of structural steel for use in design,
674 Struct. Eng. 75 (1997) 363-367.
675 [49] Arya C. Design of structural elements. London: Spon Press; 2009.

[50] R. Lu, Y. Luo, J.P. Conte, Reliability evaluation of reinforced concrete beams, Struct. Saf. 14 (1994) 277-298.

[51] EN 1993-1-1, Eurocode 3: design of steel structures – Part 1. 1: general rules and rules for buildings, Brussels: European Committee for Standardization (CEN), 2005.

[52] X. Meng, L. Gardner, A. J. Sadowski, J. M. Rotter, Elasto-plastic behaviour and design ofsemi-compact circular hollow sections. Thin-Walled Struct. 148 (2020) 106486.

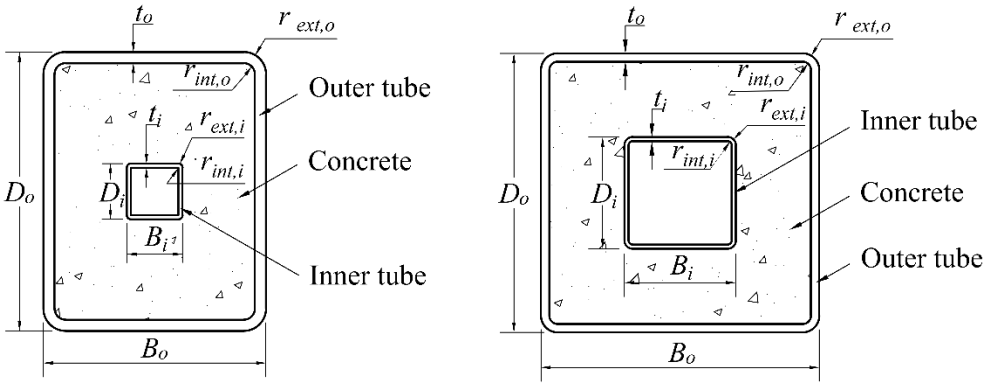

Fig. 1. Definition of symbols for CFDST specimens.

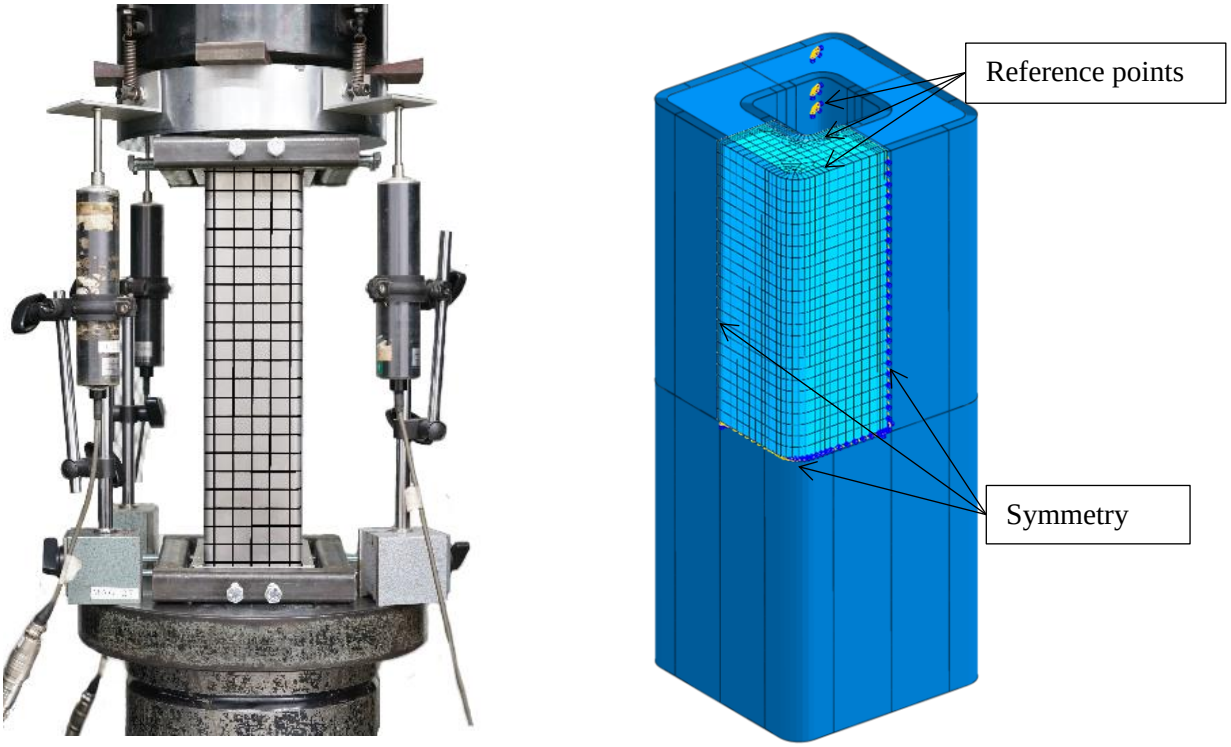

(a) Test setup. (b) FE model in ABAQUS.

Fig. 2. CFDST stub column (a) test setup and (b) FE model in ABAQUS.

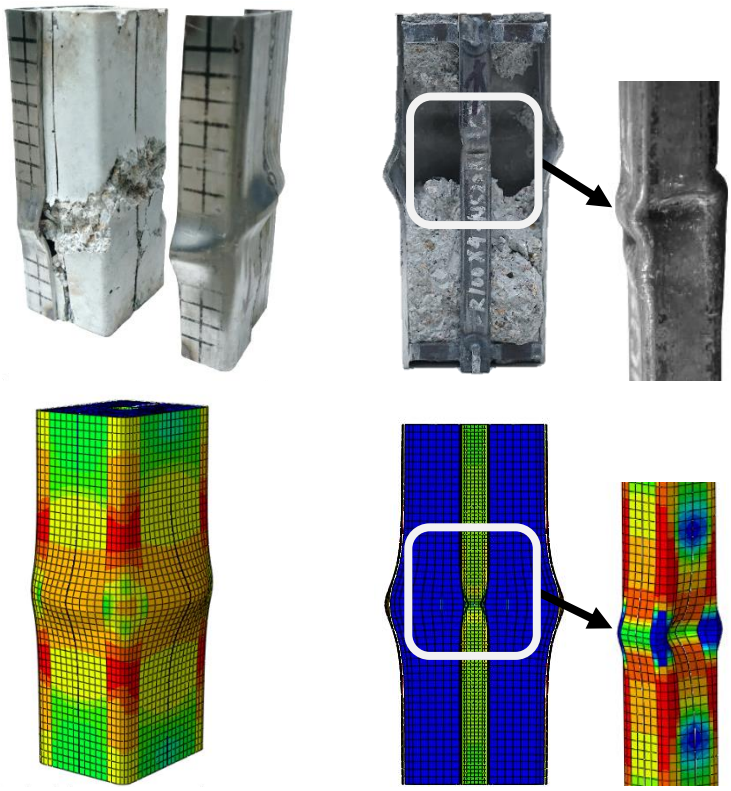

(a) Outward local buckling of outer tube. (b) Inward and outward local buckling of inner tube.

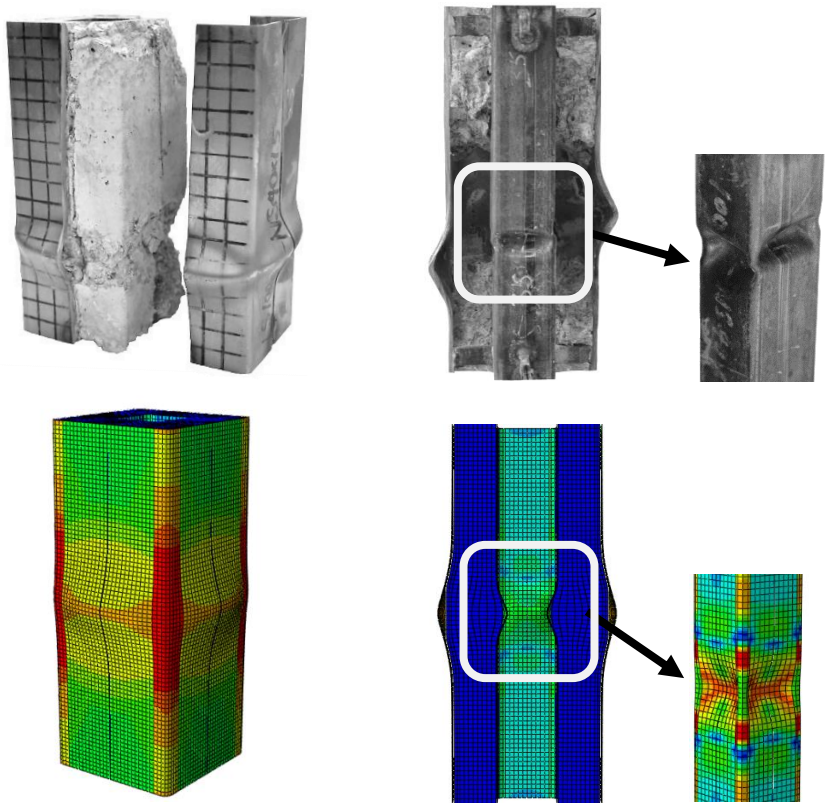

(c) Outward local buckling of outer tube. (d) Inward local buckling of inner tube.

Fig. 3. Experimental and numerical failure modes of stub columns (FR100×4-NS20×1.5-C40 (a, b) LS100×3-NS40×1.5-C40 (c, d)).

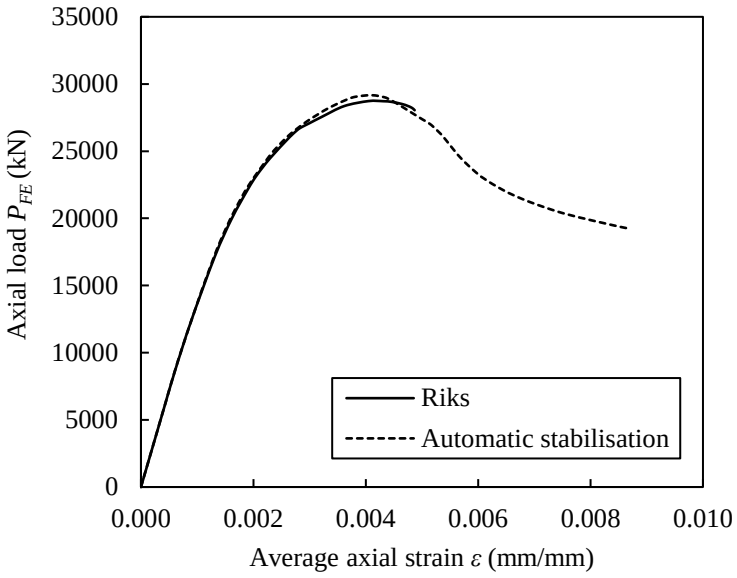

Fig. 4. Comparison of typical load–deformation responses generated from Riks and automatic stabilisation schemes.

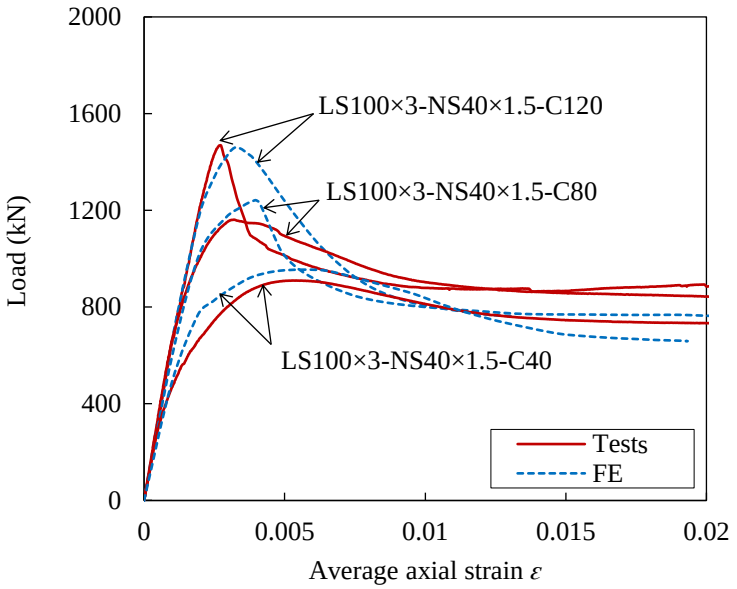

Fig. 5. Comparisons of test and FE load–average axial strain curves.

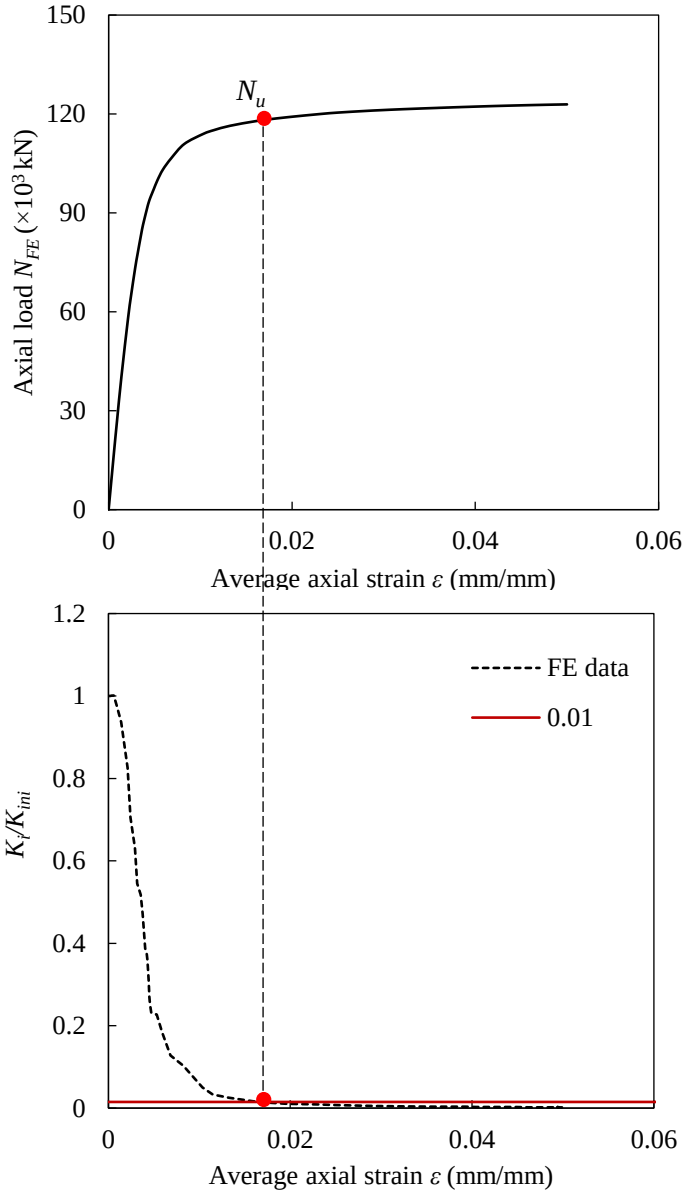

Fig. 6. Definition of ultimate axial compressive resistance when peak load was not attained in FE simulation.

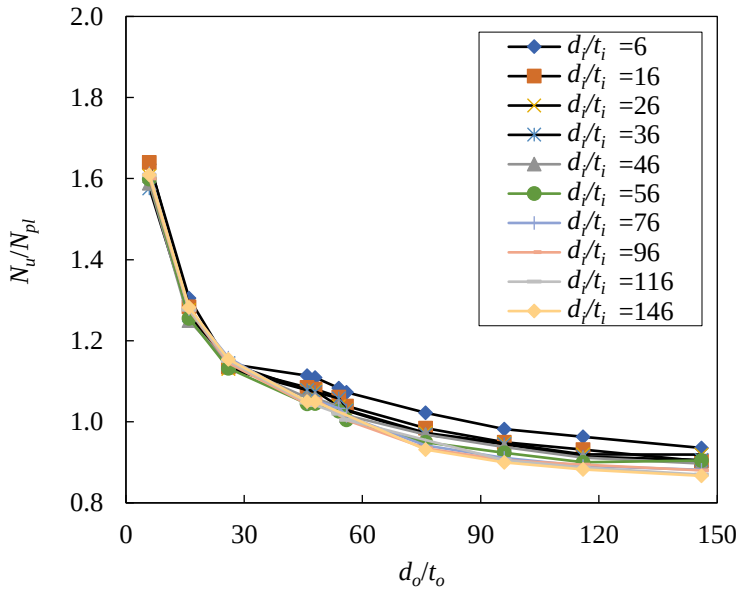

Fig. 7. Influence of outer tube slenderness on normalised resistance of studied CFDST cross-sections.

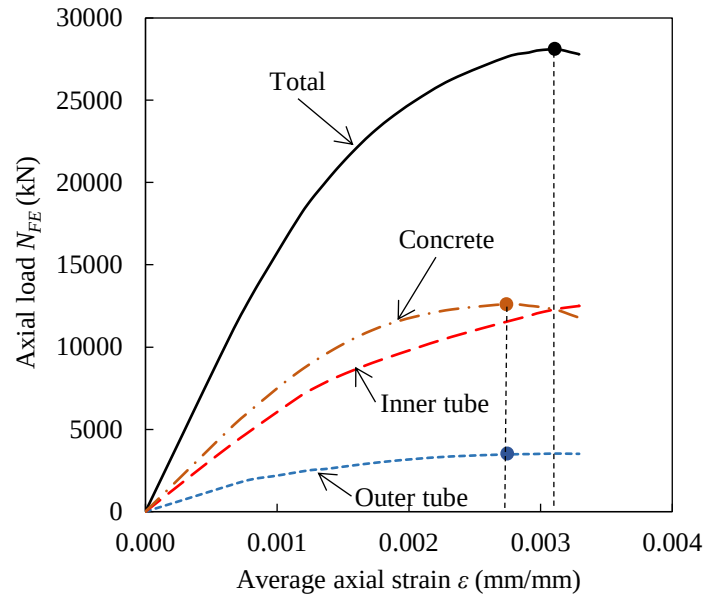

(a) Specimen LS600×5-NS300×10-C40.

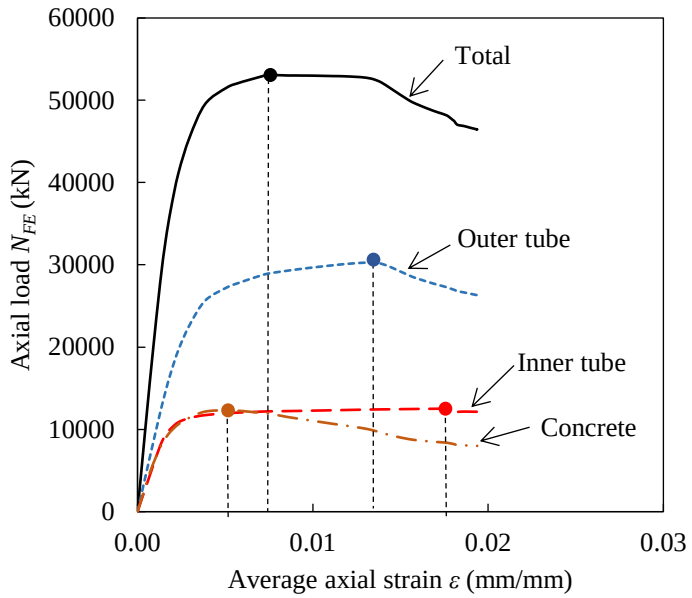

(b) Specimen LS600×20-NS300×10-C40.

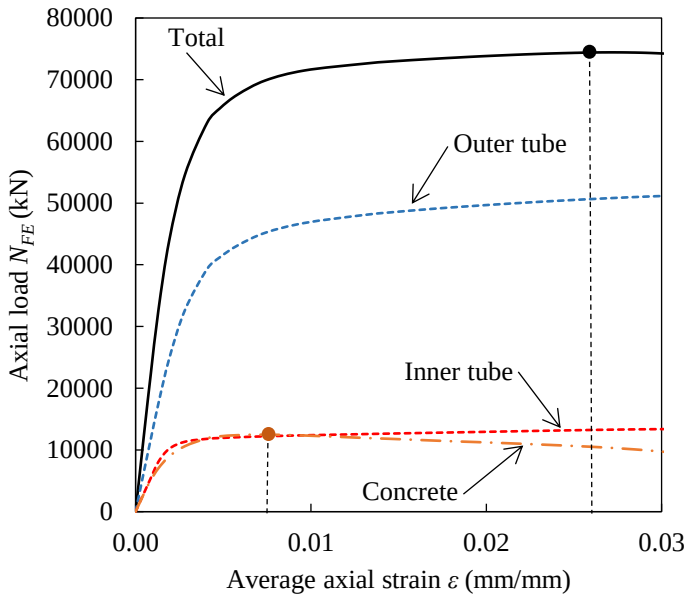

(c)Specimen LS600×30-NS300×10-C40.

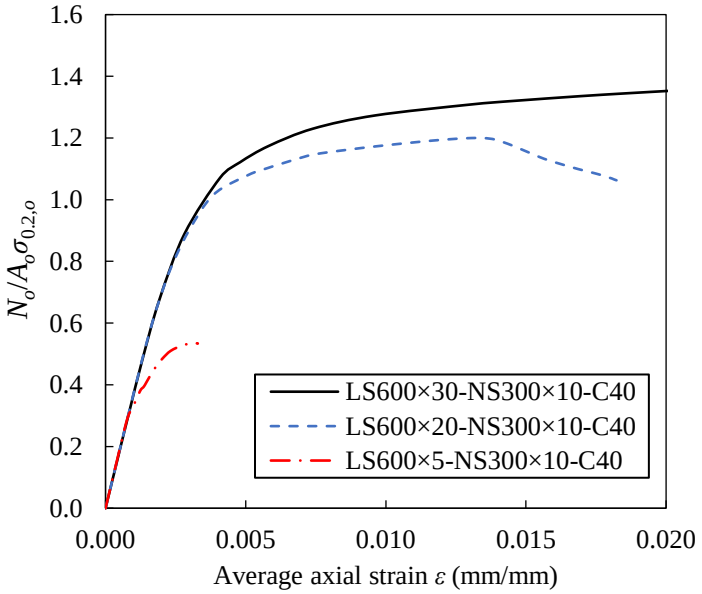

(d) Performance of outer tubes.

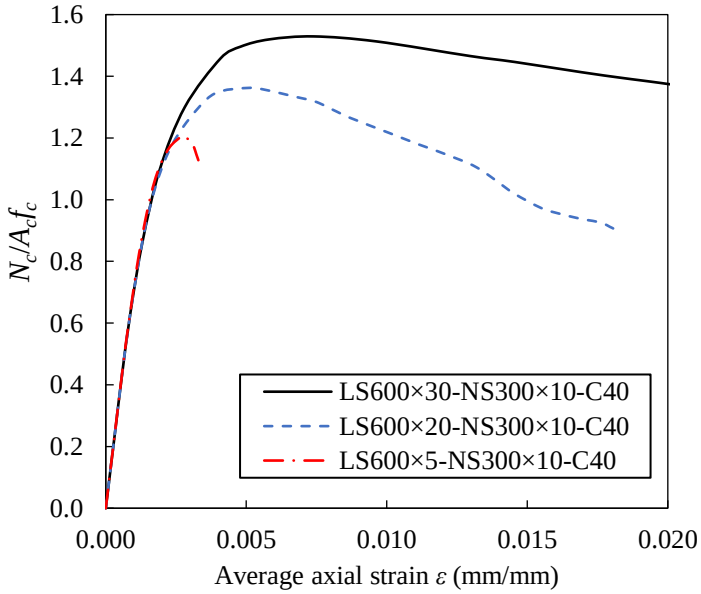

(e) Performance of concrete.

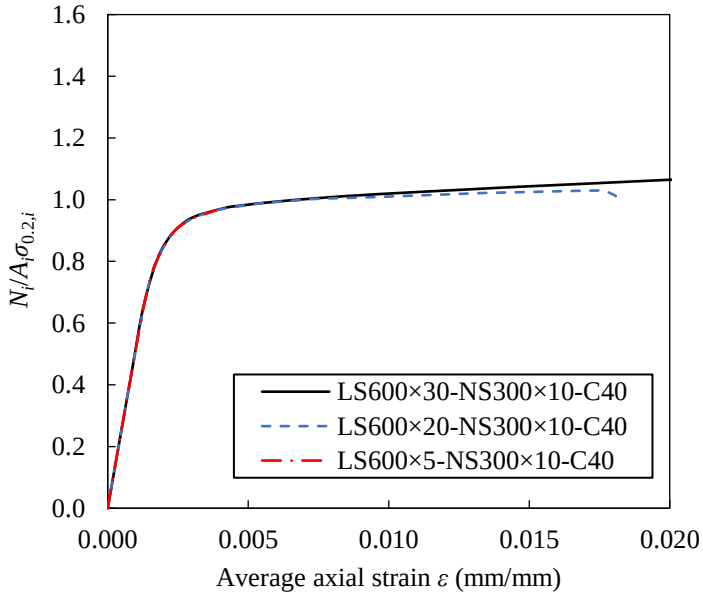

(f) Performance of inner tubes.

Fig. 8. Comparisons of CFDST specimens with varying outer tube local slendernesses.

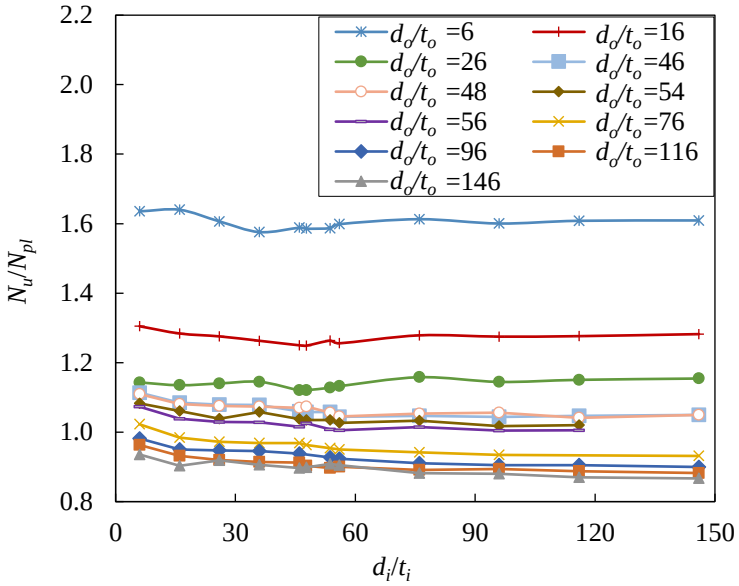

Fig. 9. Influence of inner tube slenderness on normalised load-carrying capacity of studied CFDST sections.

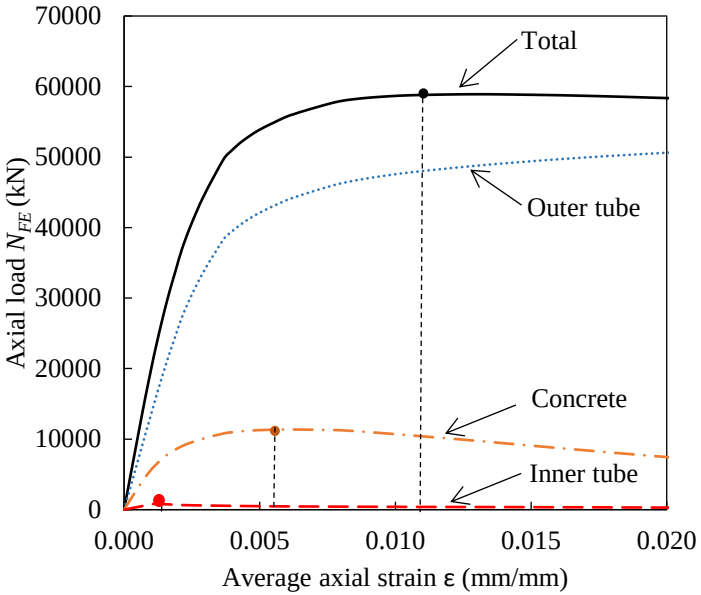

(a) Specimen LS600×30-NS300×3-C40.

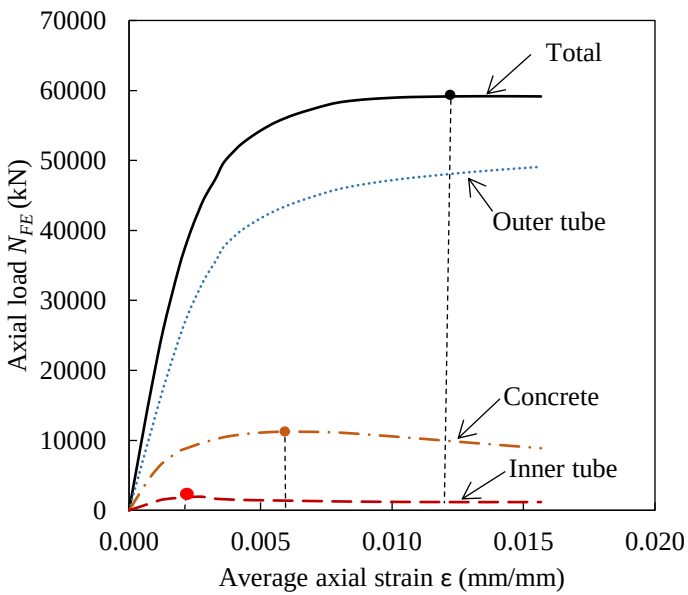

(b) Specimen LS600×30-NS300×5-C40.

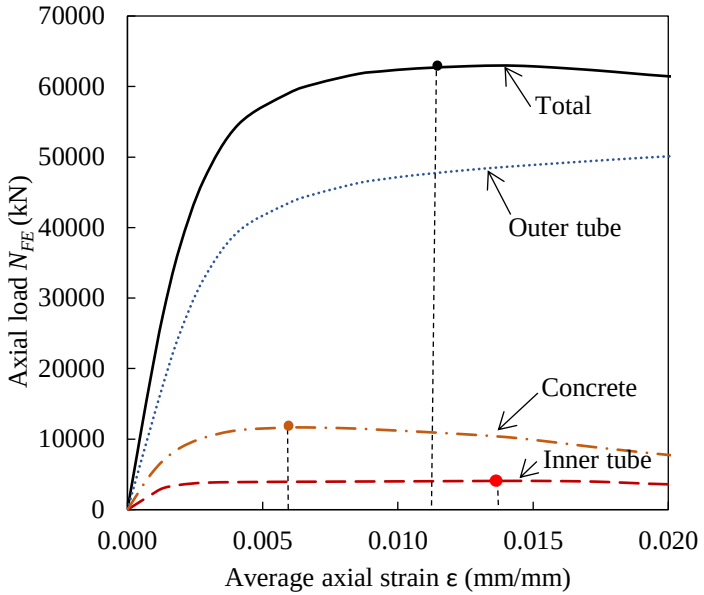

(c)Specimen LS600×30-NS300×10-C40.

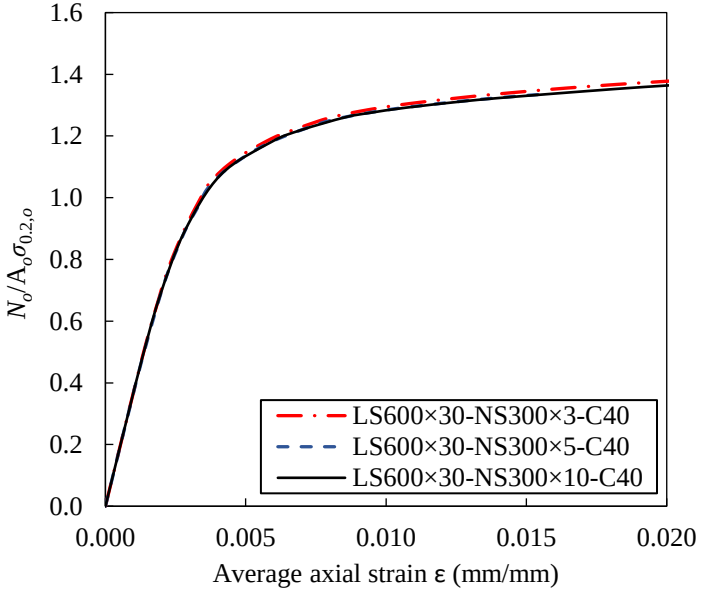

(d) Performance of outer tubes.

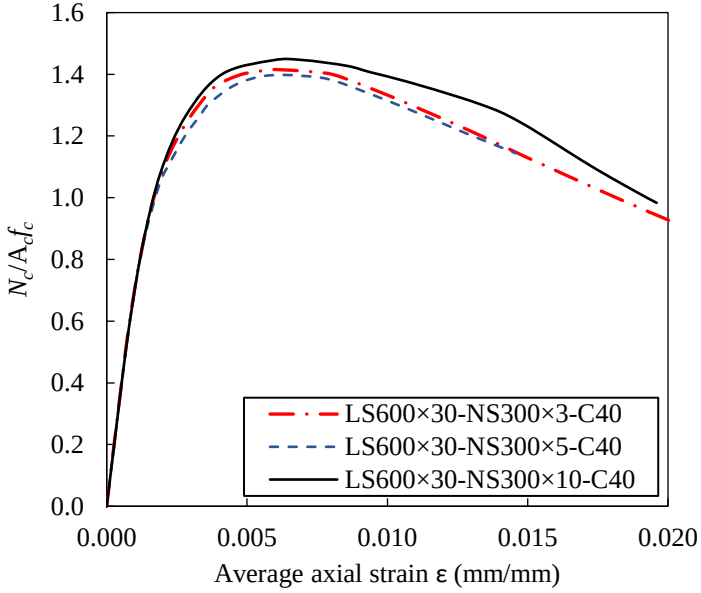

(e) Performance of concrete.

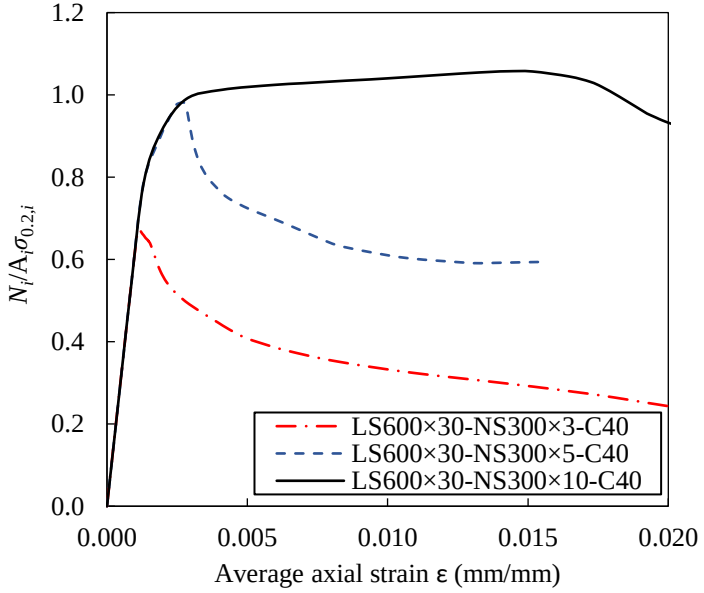

(f) Performance of inner tubes.

Fig. 10. Comparisons of CFDST specimens with varying inner tube local slendernesses.

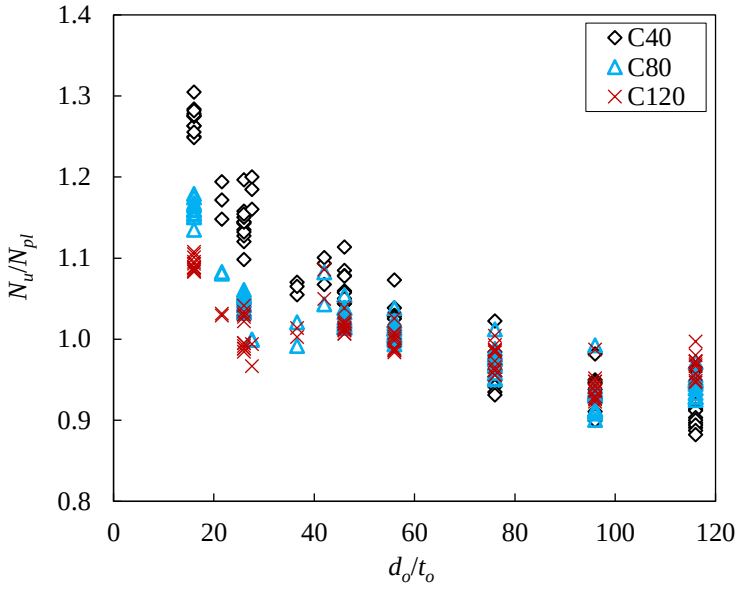

Fig. 11. Influence of concrete grade on normalised load-carrying capacity of studied CFDST sections.

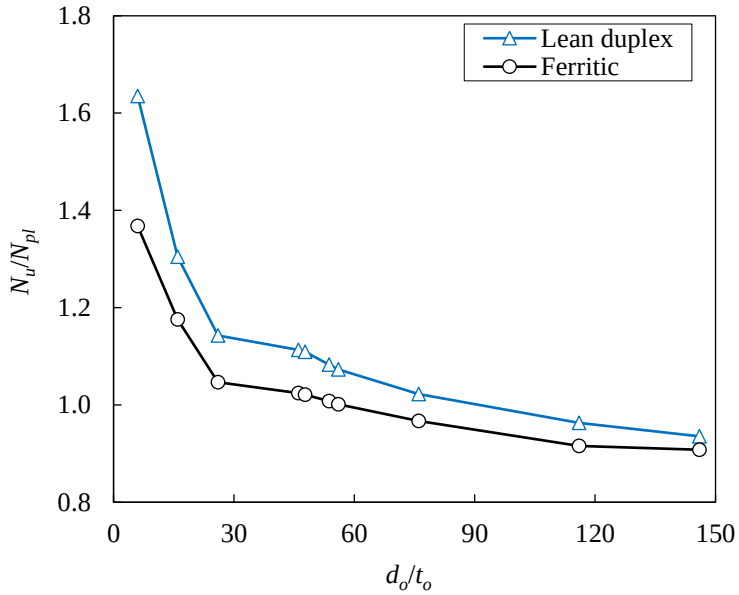

(a) Comparisons of CFDST specimens of two different stainless steel grades.

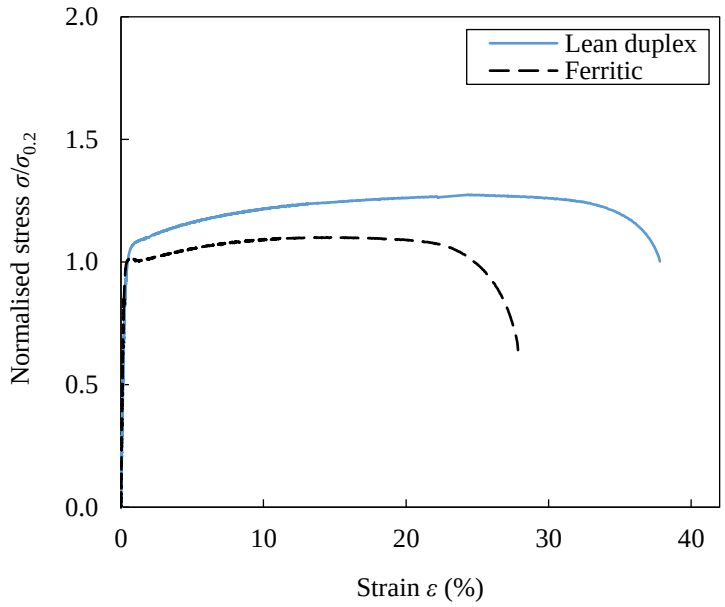

(b) Normalised material properties of lean duplex and ferritic stainless steel.

Fig. 12. Influence of stainless steel grade on normalised load-carrying capacity of studied CFDST sections.

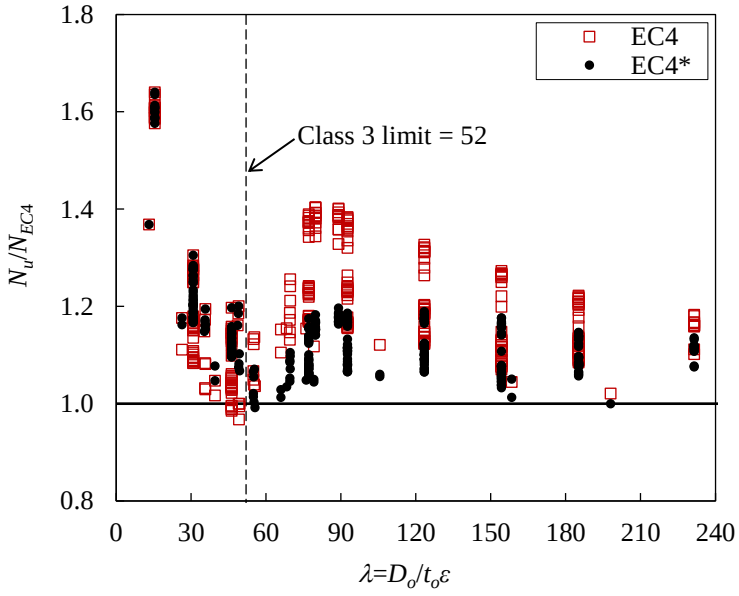

Fig. 13. Comparisons of test and FE results with strength predictions from EC4.

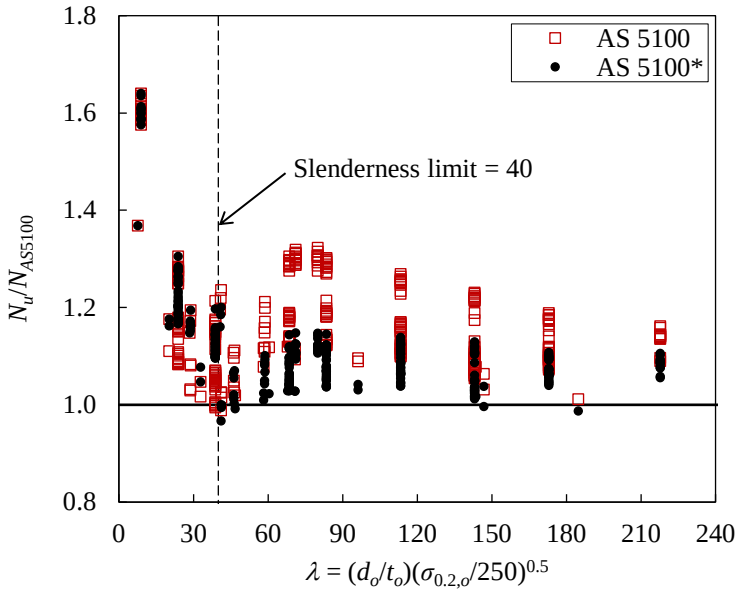

Fig. 14. Comparisons of test and FE results with strength predictions from AS 5100.

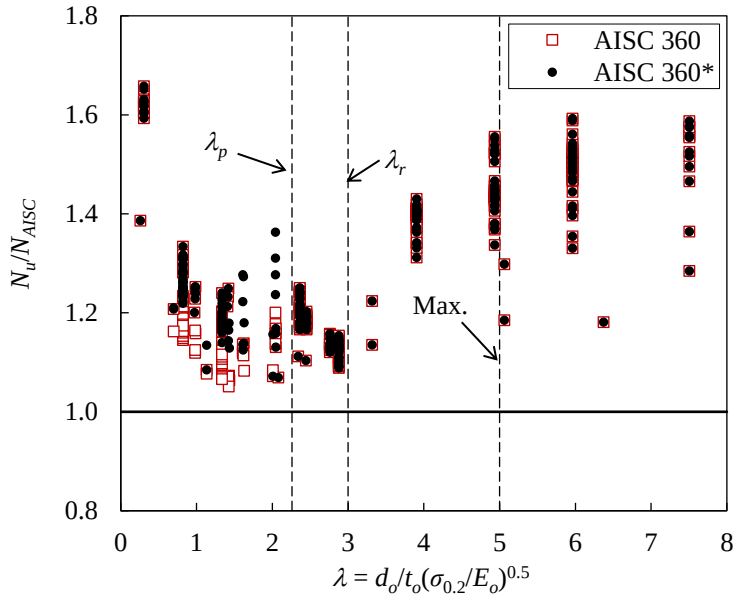

Fig. 15. Comparisons of test and FE results with strength predictions from AISC 360.

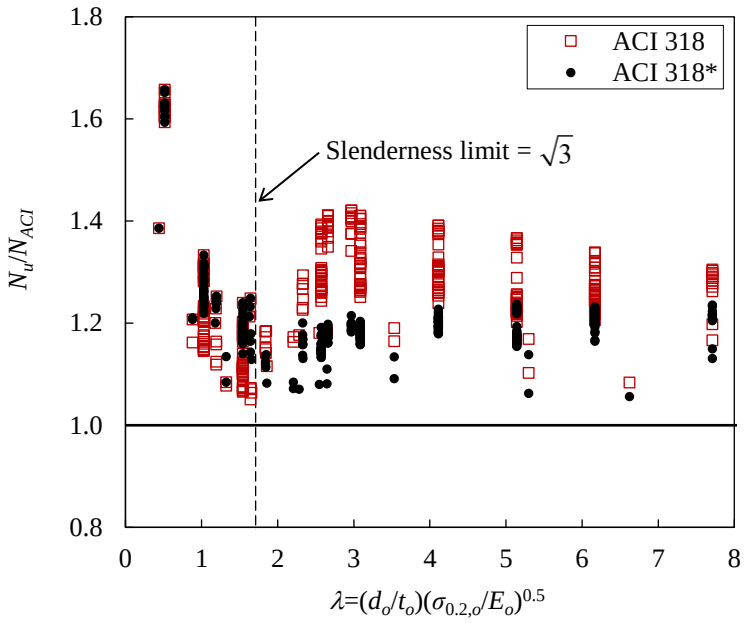

Fig. 16. Comparisons of test and FE results with strength predictions from ACI 318.

Table 1. Summary of experimental results on CFDST stub columns [10] and FE validation.

Specimen	D_o/t_o	D_i/t_i	$\sigma_{0.2,o}$ (MPa)	$\sigma_{0.2,i}$ (MPa)	f_c (MPa)	N_{exp} (kN)	N_{FE} (kN)	N_{FE}/N_{exp}
LR150×3-NS20×2.5-C40	48.6	7.7	475	468	41.8	1223	1313	1.07
LR150×3-NS20×2.5-C40R	48.6	7.7	475	468	41.8	1255	1313	1.05
LR150×3-NS20×2.5-C80	48.5	7.7	475	468	81.6	1681	1645	0.98
LR150×3-NS20×2.5-C120	48.4	7.7	475	468	115.9	1996	1963	0.98
LR150×3-NS20×1.5-C40	48.6	12.9	475	357	41.8	1216	1267	1.04
LR150×3-NS20×1.5-C80	48.5	13.2	475	357	81.6	1577	1594	1.01
LR150×3-NS20×1.5-C120	48.5	13.3	475	357	115.9	2019	1928	0.95
LS100×3-NS40×4-C40	31.8	10.4	556	404	41.8	1420	1354	0.95
LS100×3-NS40×4-C40R	31.7	10.4	556	404	41.8	1401	1354	0.97
LS100×3-NS40×4-C80	32.1	10.3	556	404	81.6	1464	1561	1.07
LS100×3-NS40×4-C120	31.9	10.4	556	404	115.9	1706	1774	1.04
LS100×3-NS40×1.5-C40	31.6	28.4	556	324	41.8	1209	1193	0.99
LS100×3-NS40×1.5-C80	31.8	28.1	556	324	81.6	1323	1401	1.06
LS100×3-NS40×1.5-C120	31.8	28.1	556	324	115.9	1516	1621	1.07
FR120×3-NS20×2.5-C40	41.9	7.7	401	468	41.8	910	954	1.05
FR120×3-NS20×2.5-C80	42.1	7.5	401	468	81.6	1161	1242	1.07
FR120×3-NS20×2.5-C120	41.7	7.7	401	468	115.9	1469	1460	0.99
FR120×3-NS20×1.5-C40	41.7	13.3	401	357	41.8	856	892	1.04
FR120×3-NS20×1.5-C40R	41.6	13.2	401	357	41.8	864	892	1.03
FR120×3-NS20×1.5-C80	41.7	13.1	401	357	81.6	1155	1196	1.04
FR120×3-NS20×1.5-C120	41.8	13.2	401	357	115.9	1409	1427	1.01
FR100×4-NS20×2.5-C40	26.1	13.1	439	468	41.8	1030	1036	1.01
FR100×4-NS20×2.5-C80	26.4	13.4	439	468	81.6	1235	1248	1.01
FR100×4-NS20×2.5-C120	26.4	13.4	439	468	115.9	1398	1427	1.02
FR100×4-NS20×1.5-C40	26.4	13.4	439	357	41.8	1015	990	0.98
FR100×4-NS20×1.5-C40R	26.3	13.1	439	357	41.8	999	990	0.99
FR100×4-NS20×1.5-C80	26.4	13.5	439	357	81.6	1191	1201	1.01
FR100×4-NS20×1.5-C120	26.3	13.1	439	357	115.9	1359	1386	1.02
Mean								1.02
COV								0.035
Max.								1.06
Min.								0.95

Table 2. Ranges of variation of parameters for the parametric study.

d_o/t_o	d_i/t_i	$\sigma_{0.2,o}$ (MPa)	$\sigma_{0.2,i}$ (MPa)	f_c (MPa)
6, 16, 26, 46, 48, 54, 56 76, 96, 116, 146	6, 16, 26, 36, 46 56, 76, 96, 116, 146	401, 556	404	40, 80, 120

Table 3. Code limits on cross-sectional slendernesses and material strengths.

Design codes	Limitations of cross-sectional slenderness		$\sigma_{0.2}$	f_c
	Original	Normalised slenderness limits	(MPa)	(MPa)
EN 1994-1-1	$D_o/t_o \le 52\sqrt{\frac{235}{\sigma_{0.2,o}}\frac{E_o}{210000}}$	$(D_o/t_o)\sqrt{\frac{210000}{E_o}\frac{\sigma_{0.2,o}}{235}} \le 52$	235–460	20–50
AS 5100	$\lambda_e = \frac{d_o}{t_o}\sqrt{\frac{\sigma_{0.2,o}}{250}} \le 40$	$\frac{d_o}{t_o}\sqrt{\frac{\sigma_{0.2,o}}{250}} \le 40$	230–400	25–65
AISC 360	$\lambda_p = \frac{d_o}{t_o} \le 2.26\sqrt{\frac{E_o}{\sigma_{0.2,o}}}$	$\frac{d_o}{t_o}\sqrt{\frac{\sigma_{0.2,o}}{E_o}} \le 2.26$	≤ 525	21–70
ACI 318	$t_o \ge D_o\sqrt{\frac{\sigma_{0.2,o}}{3E_o}}$	$(D_o/t_o)\sqrt{\frac{\sigma_{0.2,o}}{E_o}} \le \sqrt{3}$	≤ 345	≥ 17.2

Table 4. Overall comparison of test and FE axial compressive strengths with predicted strengths.

No. of tests: 28 No. of FE modelling: 311	N_u/N_{EC4}	N_u/N_{EC4*}	N_u/N_{AS5100}	$N_u/N_{AS5100*}$	N_u/N_{AISC}	N_u/N_{AISC*}	N_u/N_{ACI}	N_u/N_{ACI*}
Mean	1.20	1.14	1.17	1.12	1.27	1.29	1.27	1.21
COV	0.108	0.093	0.100	0.100	0.131	0.121	0.086	0.076

Table 5. Comparison of Test and FE strengths with design predictions for specimens falling within their respective codified slenderness limits.

f_c		Ratio of test-to-predicted strengths							
(MPa)		N_u/N_{EC4}	N_u/N_{EC4*}	N_u/N_{AS5100}	$N_u/N_{AS5100*}$	N_u/N_{AISC}	N_u/N_{AISC*}	N_u/N_{ACI}	N_u/N_{ACI*}
40	Mean	1.20	1.20	1.20	1.20	1.24	1.24	1.24	1.24
	COV	0.060	0.060	0.060	0.060	0.054	0.054	0.055	0.055
80	Mean	1.09	1.15	1.09	1.15	1.15	1.21	1.15	1.21
	COV	0.055	0.047	0.055	0.047	0.049	0.040	0.049	0.040
120	Mean	1.04	1.15	1.04	1.15	1.12	1.22	1.12	1.22
	COV	0.044	0.032	0.044	0.032	0.040	0.025	0.040	0.025

Table 6. Comparison of test and FE axial compressive strengths with design predictions for specimens exceeding their respective codified slenderness limits.

Parameters	Ratio of test-to-predicted strengths					
	N_u/N_{EC4}	N_u/N_{EC4*}	N_u/N_{AS5100}	$N_u/N_{AS5100*}$	N_u/N_{ACI}	N_u/N_{ACI*}
Mean	1.21	1.10	1.17	1.07	1.29	1.18
COV	0.083	0.042	0.069	0.036	0.053	0.029

Table 7. Reliability analysis results calculated according to EN 1990 [46].

Design code	Sample type	Sample number	$k_{d,n}$	b	V_δ	Required value of γ_{M0}	Target value of γ_{M0}
EC4	Test+FE	28+311	3.119	1.20	0.111	1.00	1.00
EC4*	Test+FE	28+311	3.119	1.14	0.088	0.99	1.00
AS 5100	Test+FE	28+311	3.119	1.17	0.100	0.94	1.00
AS 5100*	Test+FE	28+311	3.119	1.12	0.095	0.98	1.00
AISC 360	Test+FE	28+311	3.119	1.27	0.114	1.15	1.33
AISC 360*	Test+FE	28+311	3.119	1.29	0.106	1.11	1.33
ACI 318	Test+FE	28+311	3.119	1.27	0.092	1.09	1.54
ACI 318*	Test+FE	28+311	3.119	1.21	0.073	1.10	1.54